International Journal of Bifurcation and Chaos, Vol. 6, No. 11 (1996) 2015–2030

ON DYNAMICAL SYSTEMS GENERATED BY TWO ALTERNATING VECTOR FIELDS

A. KLÍČ and P. POKORNÝ
Department of Mathematics, Department of Chemical Engineering,
Prague Institute of Chemical Technology,
Technická 5, 166 28 Prague, Czech Republic

Received September 28, 1995; Revised January 21, 1996

Dynamical systems with time evolution determined by two alternating vector fields are investigated both analytically and numerically. When the two vector fields are related by an involutory diffeomorphism G then the fixed points of G (either isolated or non-isolated) are shown to give rise to branches of periodic solutions of the resulting non-autonomous system. The method of averaging is used for small switching periods. Detailed numerical study of both conservative ("blinking vortex") and dissipative ("blinking nodes", "blinking cycles" and "blinking Lorenz") systems shows that the technique of blinking can be used to initiating and controlling of chaos.

1. Introduction

In many applications the time evolution of a system is determined by two (or more) alternating dynamics. Such "kicked" systems arise naturally at the modeling of a tubular catalytic reactor with flow reversal, see for example [Řeháček *et al.*, 1992], at the modeling of kicked rotator, see [Chirikov, 1979] or in the case of blinking vortex flow, see [Ottino, 1989].

In this paper a kind of kicked system is investigated, which is described by a non-autonomous periodic system of ODE of the form

$$\dot{x} = \mathbf{v}(x) + r_p(t)(\mathbf{w}(x) - \mathbf{v}(x)), \qquad (1)$$

where $r_p(t) = 0$ for $t \in [0, p]$, $r_p(t) = 1$ for $t \in (p, 2p)$ and $r_p(t)$ is $2p-$periodic function; the two vector fields $\mathbf{v}$ and $\mathbf{w}$, related by involutory diffeomorphism G, alternately operate on the phase space. Once we fix the switching period p, we obtain a piecewise continuous dynamical system.

The contents of this paper are as follows. In Sec. 2 basic notions and definitions are given. The correspondence between the system (1) and a system with impulses is reminded. Section 3 deals with the existence of periodic solutions of Eq. (1). In Sec. 4 the method of averaging is investigated. Section 5 contains several results of numerical experiments. Namely the "blinking nodes" system where the vector field $\mathbf{v}$ has a single point attractor to illustrate the method of averaging, the "blinking cycles" system where the vector field $\mathbf{v}$ has a stable limit cycle. Detailed numerical study reveals complex dynamical behavior including the Feigenbaum cascade. The case when the vector field $\mathbf{v}$ has a chaotic attractor is also studied, showing, that for some values of the switching period p, the chaos persists while for other values the system has a single-point attractor. This way, the blinking technique can be used either for initiating or controlling chaos. The following surveys on controlling chaos, which is closely related to this paper, may be found in

E-mail: Pavel.Pokorny@vscht.cz

[Chen & Dong, 1993; Ogorzalek, 1993; Shinbrot *et al.*, 1993]. As an example of conservative system the "blinking vortex" system is studied. In Appendix A the Palmer's theorem, used in Sec. 3, is repeated for the convenience of the reader. In Appendix B the first integral for the averaged "blinking vortex" system is derived.

2. Preliminaries

Consider a sufficiently smooth vector field $\mathbf{v}$ on R^n, generating a global phase flow

$$\varphi : R \times R^n \to R^n$$

(that is a 1-parameter subgroup of diffeomorphisms φ^t, $t \in R$).

Let us further consider an involutory diffeomorphism G satisfying

$$G \circ G = \mathrm{Id} \quad \text{i.e.} \quad G^{-1} = G$$

and the G-related vector field

$$\mathbf{w} = G_*(\mathbf{v}),$$
$$\text{i.e.} \quad \mathbf{w}(x) = \mathrm{D}_x G(G^{-1}(x)) \cdot \mathbf{v}(G^{-1}(x)),$$

where $\mathrm{D}_x G(G^{-1}(x))$ denotes the Jacobi matrix of G at the point $G^{-1}(x)$.

We shall denote the flow of the vector field $\mathbf{w}$ by ψ^t. As $\mathbf{w}$ is G-related with $\mathbf{v}$,

$$\psi^t = G \circ \varphi^t \circ G. \tag{2}$$

Consider a $2p$-periodic function $r_p(t)$ defined by

$$r_p(t) = \begin{cases} 0 & \text{for} \quad t \in [0, p] \\ 1 & \text{for} \quad t \in (p, 2p). \end{cases} \tag{3}$$

Then the following $2p$-periodic non-autonomous system of ODE's

$$\dot{x} = \mathbf{f}(x, t) = \mathbf{v}(x) + r_p(t)(\mathbf{w}(x) - \mathbf{v}(x)) \tag{4}$$

describes the system with two different alternating dynamics.

Let us denote $\Phi(t; 0, x_0)$ as the solution of (4), satisfying the initial condition $\Phi(0; 0, x_0) = x_0$. This solution can be expressed for $t \in [0, 2p]$ in the form

$$\Phi(t; 0, x_0) = \begin{cases} \varphi^t(x_0) & \text{for} \quad t \in [0, p] \\ \psi^{t-p}(\varphi^p(x_0)) & \text{for} \quad t \in (p, 2p). \end{cases} \tag{5}$$

Let us denote

$$P(x) = \Phi(2p; 0, x). \tag{6}$$

Then the mapping $P : R^n \to R^n$ is a period map (also called a stroboscopic map) for the system (4) and P is a differentiable mapping.

The relation (5) yields

$$P = \psi^p \circ \varphi^p \tag{7}$$

and with respect to (2) we obtain

$$P = G \circ \varphi^p \circ G \circ \varphi^p. \tag{8}$$

Let us denote

$$H = G \circ \varphi^p, \tag{9}$$

then

$$P = H \circ H = H^2. \tag{10}$$

Remark. With respect to the relation (8), the system (4) can also be treated as a system with impulses:

$$\dot{x} = \mathbf{v}(x), \quad t \neq \tau_k = kp, \quad k \in N,$$
$$x(\tau_k - 0) = x(\tau_k), \quad x(\tau_k + 0) = G(x(\tau_k)).$$

3. Periodic Solutions

3.1. *Isolated fixed points*

In [Klíč & Řeháček, 1994], the following theorem has been proved:

Theorem 1. *Let x_0 be an isolated fixed point of G. Then there is $\varepsilon > 0$, such that the system (4) has a $2p$-periodic solution for each $p \in (0, \varepsilon)$ and if γ_p is a solution curve of the corresponding $2p$-periodic solution, then $\gamma_p \to x_0$ as $p \to 0$ in the sense of Hausdorff metric.*

That means that the periodic solution curves of (4) bifurcate from isolated fixed points x_0 analogously to Hopf bifurcation.

Proof. The periodic solution of (4) corresponds to the fixed point of period mapping P and hence to the fixed point of the mapping H. If $\hat{x}$ is a fixed point of H, i.e. $H(\hat{x}) = \hat{x}$, then

$$\varphi^p(\hat{x}) = G(\hat{x}).$$

We set

$$F(x, p) = \varphi^p(x) - G(x) \tag{11}$$

and solve

$$F(x, p) = 0 \tag{12}$$

If $(\hat{x}, p)$ is a solution of Eq. (12) then the point $\hat{x}$ is a fixed point of the mapping H.

So let x_0 be a fixed point of the diffeomorphism G. Then $(x_0, 0)$ is a solution of Eq. (12), since

$$F(x_0, 0) = \varphi^0(x_0) - G(x_0) = x_0 - x_0 = 0\,.$$

If $\mathrm{D}_x F(x_0, 0)$ is a regular matrix, then according to the Implicit Function Theorem, there is an $\varepsilon > 0$ such that for every $p \in (-\varepsilon, \varepsilon)$ there exists $\hat{x}(p)$, satisfying $F(\hat{x}(p), p) = 0$. The matrix

$$\begin{aligned}\mathrm{D}_x F(x_0, 0) &= \frac{\partial \varphi^0}{\partial x}(x_0) - \mathrm{D}_x G(x_0) \\ &= I - \mathrm{D}_x G(x_0)\end{aligned} \tag{13}$$

(I being the unit matrix) is regular if and only if 1 is not an eigenvalue of $\mathrm{D}_x G(x_0)$, which is exactly when x_0 is an isolated fixed point of G.

3.2. *Non-isolated fixed points*

Now, the natural question arises, what happens if the fixed point x_0 is not isolated.

Let us denote

$$\mathcal{M} = \{x \in R^n,\ G(x) = x\} \tag{14}$$

and suppose $\mathcal{M}$ is a manifold, $\dim \mathcal{M} = k < n$, $k > 0$. If $x_0 \in \mathcal{M}$, then x_0 is not an isolated fixed point of G.

As in the case of Theorem 1, we shall solve Eq. (12), but when the fixed point x_0 is not isolated, the Implicit Function Theorem cannot be used. The useful tool for investigation of Eq. (12) in this setting is the K. J. Palmer's Theorem 4.1 from [Palmer, 1984]. For the convenience of the reader, we recall this theorem in Appendix A in a slightly modified form.

Now we shall use the theorem to solve Eq. (12). We have $\mathcal{E} = \mathcal{F} = R^n$, hence the linear operator

$$L = F_x(x_0, 0) = I - G_x(x_0) \tag{15}$$

is Fredholm with index zero. (The $G_x(x_0)$ denotes the Jacobi matrix of G at the point $x_0 \in \mathcal{M}$.)

(i) It is obvious, that for $x \in \mathcal{M}$

$$F(x, 0) = \varphi^0(x) - G(x) = 0\,.$$

Further, we shall determine the kernel $\mathcal{N}(L)$. Because G is an involutory diffeomorphism and x_0 is a fixed point of G, then the matrix $G_x(x_0)$ has only eigenvalues $+1$ and -1 (from $G \circ G = \mathrm{Id}$ we obtain $G_x(G(x)) \cdot G_x(x) = I$ and for $x_0 = G(x_0)$ we have $[G_x(x_0)]^2 = I$).

Let $\mathcal{E}^+$ resp. $\mathcal{E}^-$ denote the eigenspace of the matrix $G_x(x_0)$ corresponding to the eigenvalue $+1$ resp. -1.

Then

$$\mathcal{N}(L) = \mathcal{E}^+\,, \tag{16}$$

because

$$\begin{aligned}\mathbf{h} \in \mathcal{N}(L) &\Leftrightarrow [I - G_x(x_0)]\mathbf{h} = \mathbf{0} \\ &\Leftrightarrow G_x(x_0)\mathbf{h} = \mathbf{h}\,.\end{aligned}$$

Similarly we obtain

$$\mathcal{R}(L) = \mathcal{E}^-\,. \tag{17}$$

Now we shall determine $T_{x_0}\mathcal{M}$. Let $c : R \to \mathcal{M}$, $c(0) = x_0$, be a smooth curve on $\mathcal{M}$ based at x_0. Then

$$\frac{dc}{dt}(0) = \dot{c}(0) \in T_{x_0}\mathcal{M}\,.$$

In view of the fact that $c(t) \in \mathcal{M}$ for all $t \in R$, we have

$$G(c(t)) = c(t) \tag{18}$$

for all $t \in R$. Differentiating both sides of (18) with respect to t, we obtain for $t = 0$

$$G_x(x_0)\dot{c}(0) = \dot{c}(0)\,. \tag{19}$$

From (16) and (19) we obtain

$$T_{x_0}\mathcal{M} = x_0 \oplus \mathcal{N}(L)\,.$$

So, the condition (i) in Palmer's theorem is fulfilled.

(ii) Let us determine $F_p(x_0, 0)$. We have

$$\begin{aligned}F_p(x_0, 0) &= \frac{\partial}{\partial p}(\varphi^p(x) - G(x))\Big|_{(x=x_0,\,p=0)} \\ &= \frac{\partial}{\partial p}(\varphi^p(x))\Big|_{(x=x_0,p=0)} \\ &= \mathbf{v}(\varphi^p(x))|_{(x=x_0,p=0)} = \mathbf{v}(x_0)\,.\end{aligned}$$

Hence the condition (ii) from Palmer's theorem is

$$\mathbf{v}(x_0) \in \mathcal{E}^-\,. \tag{20}$$

(iii) From the relation (13) we have

$$F_{xx}(x_0, 0) = -G_{xx}(x_0) \tag{21}$$

and differentiating the relation

$$F_p(x, p) = \mathbf{v}(\varphi^p(x))$$

with respect to x, we obtain

$$F_{px}(x_0, 0) = \frac{\partial \mathbf{v}}{\partial x}(x_0)\,. \tag{22}$$

For the sake of abbreviation we put

$$B = \frac{\partial \mathbf{v}}{\partial x}(x_0) - G_{xx}(x_0)\mathbf{u}$$

where $\mathbf{u}$ is a solution of the equation

$$L\mathbf{u} = -\mathbf{v}(x_0)\,.$$

Then the condition (iii) of Parmer's theorem implies:

$$(\mathbf{y} \in \mathcal{N}(L) = \mathcal{E}^+$$
$$\text{and} \quad B\mathbf{y} \in \mathcal{R}(L) = \mathcal{E}^-) \Rightarrow \mathbf{y} = \mathbf{0}\,.$$

Otherwise, the condition (iii) will be fulfilled if

$$B(\mathcal{E}^+) \cap \mathcal{E}^- = \{\mathbf{0}\}\,. \tag{23}$$

So we have obtained

Theorem 2. *Let $x_0 \in \mathcal{M}$. If $\mathbf{v}(x_0) \in \mathcal{E}^-$ and $B(\mathcal{E}^+) \cap \mathcal{E}^- = \{\mathbf{0}\}$, then there is $\varepsilon > 0$, such that the system (4) has a 2p-periodic solution for each $p \in (0, \varepsilon)$ and if γ_p is a solution curve of the corresponding 2p-periodic solution, then $\gamma_p \to x_0$ as $p \to 0$ in the sense of Hausdorff metric.*

3.3. *2-periodic points of H*

Until now we have investigated the existence of periodic solutions of (4) for small p, which correspond to the fixed points of the mapping $H = G \circ \varphi^p$.

The period mapping $P = H \circ H$ can have also the fixed points, arising from the two periodic orbits of the mapping H. More precisely, if the couple of the points x_1, x_2 exists such that

$$H(x_1) = x_2 \quad \text{and} \quad H(x_2) = x_1\,, \tag{24}$$

then these points x_1 and x_2 are fixed points of the period mapping P. In this way we obtain other periodic solution of (4).

The relation (24) can be rewritten in the form

$$G \circ \varphi^p(x_1) = x_2$$
$$G \circ \varphi^p(x_2) = x_1$$

or

$$\varphi^p(x_1) - G(x_2) = 0$$
$$\varphi^p(x_2) - G(x_1) = 0\,. \tag{25}$$

Let us denote

$$X = (x_1, x_2) \in R^{2n}\,,$$
$$f_1(x_1, x_2, p) = \varphi^p(x_1) - G(x_2)$$
$$f_2(x_1, x_2, p) = \varphi^p(x_2) - G(x_1)$$

and

$$F = (f_1, f_2)\,.$$

Then

$$F : R^{2n} \times R \to R^{2n}$$

and the Eq. (25) can be written in the form

$$F(X, p) = 0.$$

The solution of this equation can be again investigated using Palmer's theorem. Let

$$\tilde{\mathcal{M}} = \{(x, G(x)) \in R^{2n},\, x \in R^n\}\,,$$

that is

$$\tilde{\mathcal{M}} = \text{graph}(G)$$

is a smooth manifold, $\dim \tilde{\mathcal{M}} = n$. Considering that

$$F(X, 0) = F(x_1, x_2, 0) = (x_1 - G(x_2),\, x_2 - G(x_1))\,,$$

then

$$F(X, 0) = 0$$

for all $X \in \tilde{\mathcal{M}}$.

Further application of the Palmer's theorem is straightforward.

Remark. The above described procedure can also be used for large values of switching period p. The results of this section are demonstrated on the well-known example of blinking vortex flow in Sec. 5.

4. Averaging

In this section, the vector fields $\mathbf{v}$, $\mathbf{w}$ occurring at the right-hand side of (4), can be *arbitrary* smooth vector fields (i.e. not G-related).

If in the system (4) the time scale is changed by the relation

$$t = 2p\tau\,,$$

we obtain the system in the form

$$\dot{x} = \varepsilon \tilde{f}(x, \tau) \tag{26}$$

where

$$\varepsilon = 2p\,,$$

$$\tilde{f}(x, \tau) = \mathbf{v}(x) + \hat{r}(\tau)[\mathbf{w}(x) - \mathbf{v}(x)]$$

$$\hat{r}(\tau) = \begin{cases} 0 & \text{for } \tau \in \left[0, \frac{1}{2}\right] \\ 1 & \text{for } \tau \in \left(\frac{1}{2}, 1\right), \end{cases}$$

and

$$\hat{r}(\tau + 1) = \hat{r}(\tau)\,.$$

Then the system (26) can be treated as the system with small parameter $\varepsilon > 0$ and with 1-periodic piecewise continuous right-hand side.

Then the associated autonomous averaged system has the form

$$\dot{y} = \varepsilon \hat{f}(y) = \frac{\varepsilon}{2}[\mathbf{v}(y) + \mathbf{w}(y)]\,, \tag{27}$$

because

$$\hat{f}(y) = \int_0^1 (\mathbf{v}(y) + \hat{r}(\tau)[\mathbf{w}(y) - \mathbf{v}(y)])d\tau$$
$$= \frac{1}{2}[\mathbf{v}(y) + \mathbf{w}(y)]\,.$$

The problem of averaging for piecewise continuous right-hand side is solved in the paper by [Matveev *et al.*, 1978]. Our system (26) fulfills the conditions of Theorem 2 in [Matveev *et al.*, 1978], hence we have the following results:

Let $x(t, \varepsilon)$ denote a solution of (26) and let $y(t, \varepsilon)$ denote a solution of (27), $y(0, 1) = x_0$. Then for arbitrary $\delta > 0$, there exists $\varepsilon_0 > 0$ and $\mu > 0$ such that for every solution $x(t, \varepsilon)$ of (11) for which

$$|x(0, \varepsilon) - x_0| < \mu, \quad \varepsilon < \varepsilon_0$$

the inequality

$$|x(t, \varepsilon) - y(t, \varepsilon)| < \delta \tag{28}$$

is correct for all $t \in [0, \mathcal{O}(\frac{1}{\varepsilon})]$.

Now, let y_0 be a hyperbolic singular point of Eq. (27). Further we consider the Poincare mappings $\tilde{P}_\varepsilon$, $\hat{P}_\varepsilon$ associated with (26) and (27) respectively. The mapping $\hat{P}_\varepsilon$ has the hyperbolic fixed point y_0. With respect to (28), the inequality

$$|\tilde{P}_\varepsilon(x) - \hat{P}_\varepsilon(x)| < \delta \tag{29}$$

holds on some neighborhood $\mathcal{U}(y_0)$. Thus the mapping $\tilde{P}_\varepsilon$ is δ-close to $\hat{P}_\varepsilon$, hence the $\tilde{P}_\varepsilon$ has a fixed point, which is δ-close to y_0.

So, we can formulate the following conclusion:

Theorem 3. *If y_0 is a hyperbolic singular point of (27), then there exists $\varepsilon_0 > 0$ such that for all $0 < \varepsilon < \varepsilon_0$, the system (26) possesses a periodic solution of the same stability type as y_0, its phase curve is δ-close to y_0.*

We shall illustrate this result by the example "blinking nodes" in the next section.

5. Remarks and Examples

5.1. *Remarks*

Remark. The period mapping P is closely connected with the mapping

$$Q = \varphi^p \circ \psi^p = \varphi^p \circ G \circ \varphi^p \circ G\,. \tag{30}$$

The mappings P and Q are conjugated by the involution G, i.e.

$$Q = G \circ P \circ G\,. \tag{31}$$

However the mappings P and Q are also conjugated by the mapping φ^p, because

$$Q = \varphi^p \circ P \circ \varphi^{-p}\,. \tag{32}$$

Now, if we suppose that $\mathcal{A}$ is a *unique* attractor of the period mapping P, then the mapping Q has also a unique attractor $\mathcal{B}$ for which, with respect to the relations (31) and (32)

$$\mathcal{B} = G(\mathcal{A}) \quad \text{and} \quad \mathcal{B} = \varphi^p(\mathcal{A})\,.$$

Hence, if the period mapping P has a unique attractor $\mathcal{A}$, then this attractor must satisfy the condition

$$G(\mathcal{A}) = \varphi^p(\mathcal{A})\,. \tag{33}$$

Remark. The following question is natural: If the flow φ^t of the vector field $\mathbf{v}$ has an attractor $\mathcal{A}$ (and hence the flow ψ^t of the vector field $\mathbf{w}$ has the attractor $G(\mathcal{A})$), what can be told about the attractor of the period mapping P of the system (4)?

We shall demonstrate this problem by means of four numerical experiments in this section using [Pokorny, 1995a, 1995b, 1995c].

5.2. *"Blinking nodes"*

Let us have the vector fields

$$\mathbf{v}(x, y) = (-x + 1, -y)$$
$$\mathbf{w}(x, y) = (-x - 1, -y).$$

Their phase flows are

$$\varphi^t(x, y) = (1 + (x - 1)e^{-t}, ye^{-t})$$
$$\psi^t(x, y) = (-1 + (x + 1)e^{-t}, ye^{-t}).$$

The system (4) has the form

$$\begin{aligned} \dot{x} &= -x + 1 - 2r_p(t) \\ \dot{y} &= -y \end{aligned} \tag{34}$$

and the associated autonomous averaged system is

$$\begin{aligned} \dot{x} &= -x \\ \dot{y} &= -y \end{aligned} \tag{35}$$

with the hyperbolic (stable) singular point (0, 0). It is easy to verify that the system (34) has the periodic solution $\Phi(t; 0, x^*)$, where

$$x^* = \frac{e^{-p} - 1}{e^{-p} + 1},$$

because

$$\varphi^p(x^*, 0) = (-x^*, 0)$$

and

$$\psi^p(-x^*, 0) = (x^*, 0).$$

The phase curve of this periodic solution is the segment on the $x-$axis with end points x^* and $-x^*$, see Fig. 1. Also depicted is the phase curve of the system (34) for $p = 0.3$, starting at the point $(\frac{1}{2}, 1)$ together with the trajectory of (35), passing through the point $(\frac{1}{2}, 1)$.

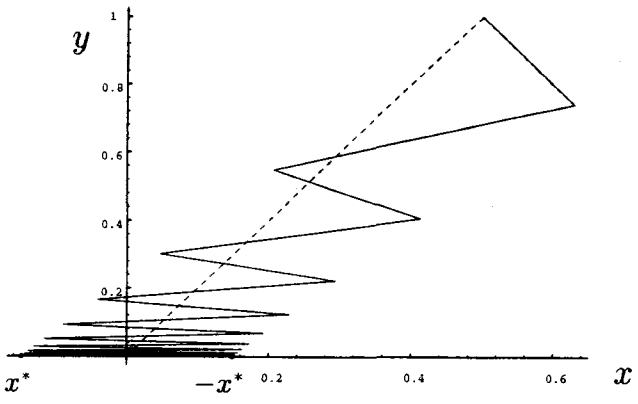

Fig. 1. Trajectory of the "blinking nodes" system (solid line) and of the corresponding averaged system (dashed line).

In this simple example, the flow φ^t of the vector field in question has a single-point attractor and the corresponding period mapping P also has a single-point attractor.

5.3. *"Blinking cycles"*

Let us consider the planar vector field

$$\mathbf{v}_\mu(x, y) = \begin{bmatrix} \mu(x-1) - y - (x-1)[(x-1)^2 + y^2] \\ (x-1) + \mu y - y[(x-1)^2 + y^2] \end{bmatrix}, \tag{36}$$

where $\mu > 0$.

The vector field $\mathbf{v}_\mu$ has a unique attractor — a stable limit cycle, centered at the point $(1, 0)$ with the radius $\sqrt{\mu}$.

Let the involution G be a linear mapping determined by the matrix

$$\begin{pmatrix} -1 & 0 \\ 0 & -1 \end{pmatrix}$$

i.e.

$$G(x, y) = (-x, -y). \tag{37}$$

Then the vector field $\mathbf{w}_\mu = G_* \mathbf{v}_\mu$ has the form

$$\mathbf{w}_\mu(x, y) = \begin{bmatrix} \mu(x+1) - y - (x+1)[(x+1)^2 + y^2] \\ (x+1) + \mu y - y[(x+1)^2 + y^2] \end{bmatrix}, \tag{38}$$

where $\mu > 0$ and the phase portraits of $\mathbf{v}_\mu$ and $\mathbf{w}_\mu$ are centrally symmetric with respect to the origin (0, 0).

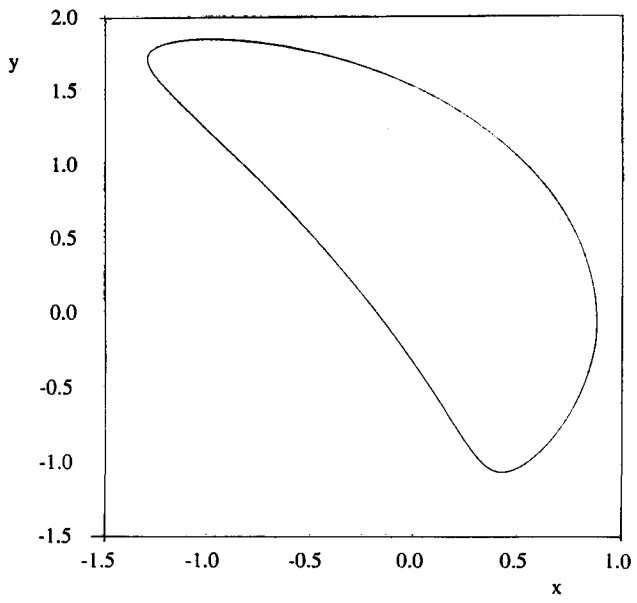

Fig. 2. The attractor of the period map of the "blinking cycles" system for $\mu = 3.5$ and $p = 0.52$ lies on a closed smooth finite-length curve. The attractor of the continuous-time system is a 2-torus.

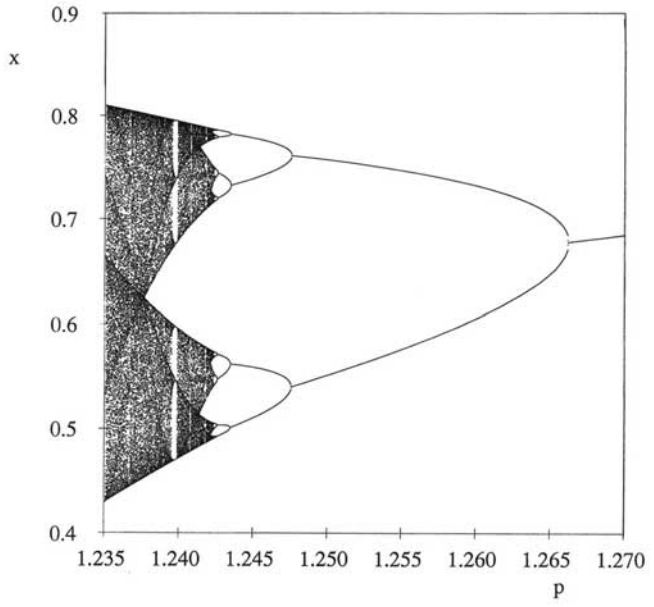

Fig. 3. Feigenbaum cascade in the "blinking cycles" system for $\mu = 3.5$. The x projection of the attractor for various values of the switching period p is plotted.

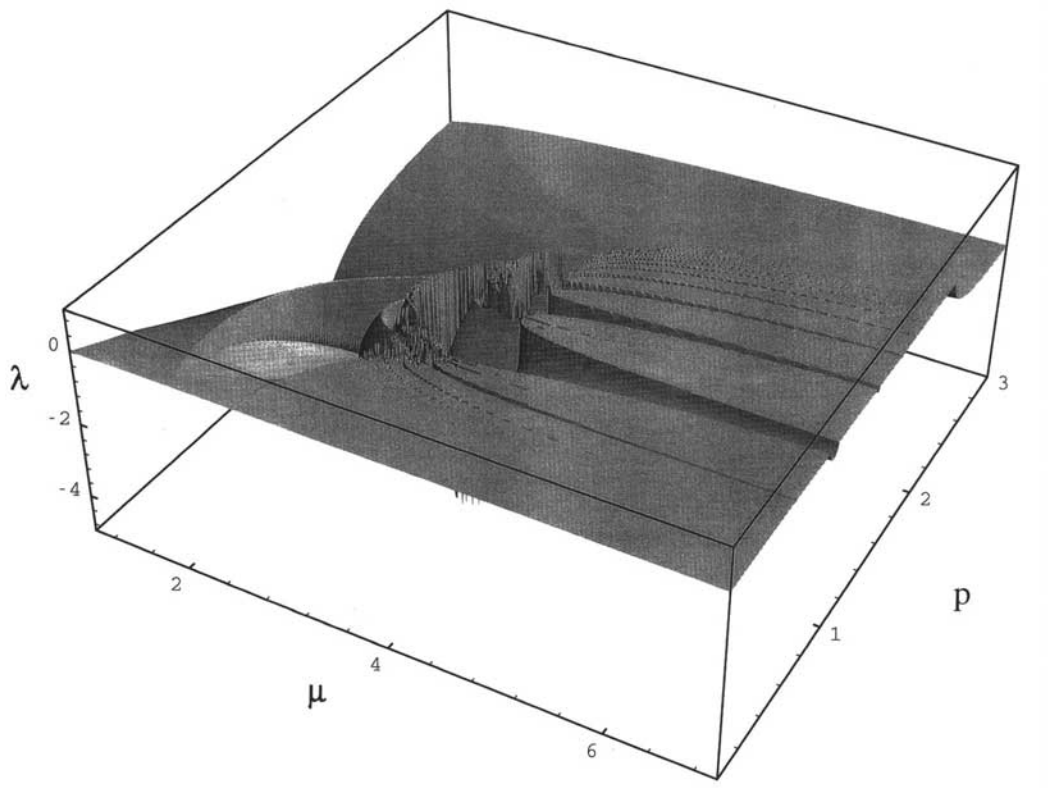

Fig. 4. The largest Lyapunov exponent λ of the period map of the "blinking cycles" system as a function of the "amplitude" parameter μ and the switching period p. For small values of μ (corresponding to large amplitudes) λ is negative and the dynamics is synchronized with the switching. For intermediate values of μ chaotic regimes appear while for large μ synchronization occurs only for narrow intervals of p resembling Arnold tongues. Tongues of higher order seem to be interrupted which is caused by the limited resolution of the grid (400×400 points yielding $\delta p \approx 0.0075$) and the small width of some tongues (below 0.001).

The origin (0, 0) is an isolated fixed point of the involution G. Now we can use the Theorem 1 or Theorem 3 to obtain the fixed point of the period mapping P for small p. By the continuation method we can obtain the dependence of this fixed point on the parameter p.

If we fix $\mu = 3.5$ then, for example, for the switching period $p \in (2, 3)$, the period mapping P has a single stable fixed point, i.e. P has a single-point attractor.

For $p = 0.52$ the simple closed curve, plotted in Fig. 2, is the attractor for the period mapping P.

For $\mu = 3.5$ and $p \in (1.24; 1.27)$ Feigenbaum period-doubling cascade leading to chaos for decreasing p is shown in Fig. 3. We note that for the same parameter values there is one more co-existing period-doubling cascade with coinciding bifurcation values. There is also the period-doubling cascade for increasing p (for p around 0.84) which co-exists with a period-3 solution with a much larger basin of attraction.

Figure 4 shows the dependence of the largest Lyapunov exponent λ on the parameters μ and p. As the distance of centers of the two blinking cycles is kept constant (equal to 2 in our example) and the radius of the cycles is $\sqrt{\mu}$, the reciprocal value of the radius $1/\sqrt{\mu}$ can be considered a mean amplitude of the forcing caused by the blinking. For small μ (large amplitude) the dynamics is synchronized with the switching (considered here as external signal). For intermediate values of μ chaos and bistability occurs. For large μ (small amplitude) the synchronization occurs only for narrow intervals of p, which form a structure resembling Arnold tongues.

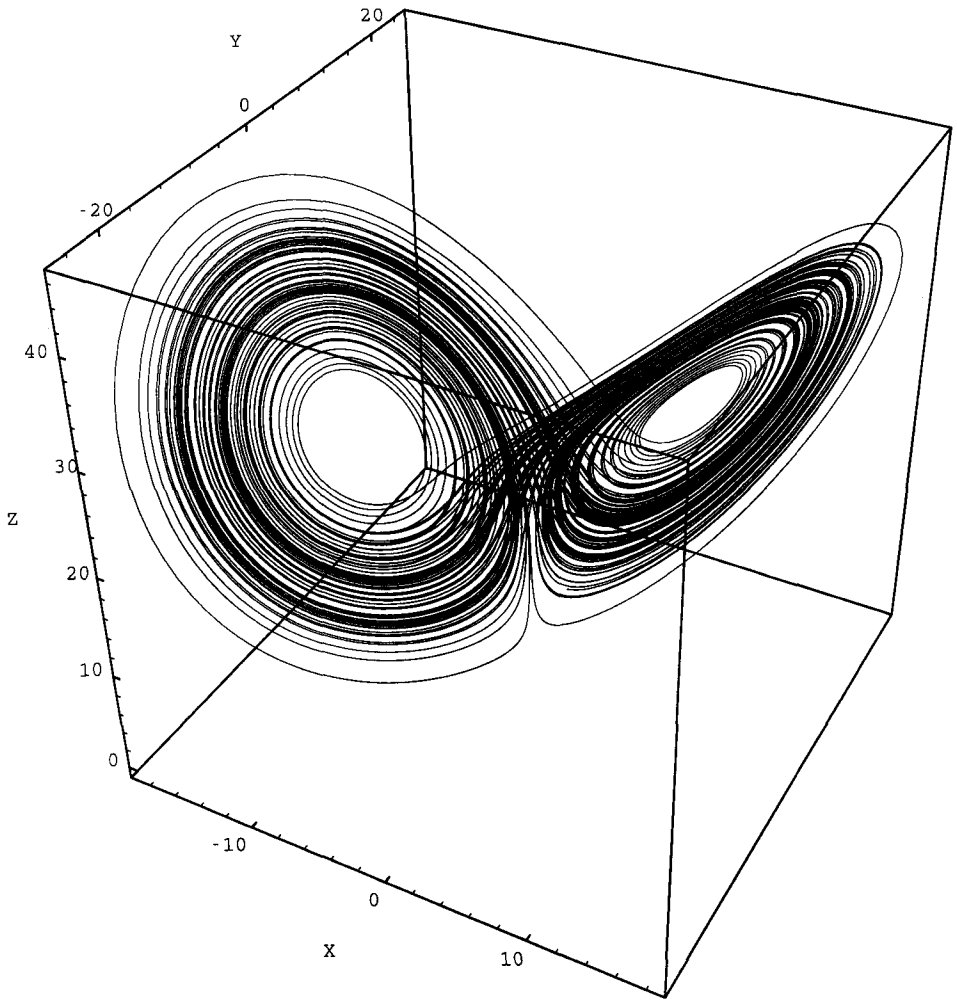

Fig. 5. The 3-D phase portrait of the Lorenz system. Sampling period is $T_S = 0.003$, the number of samples is $n = 20000$.

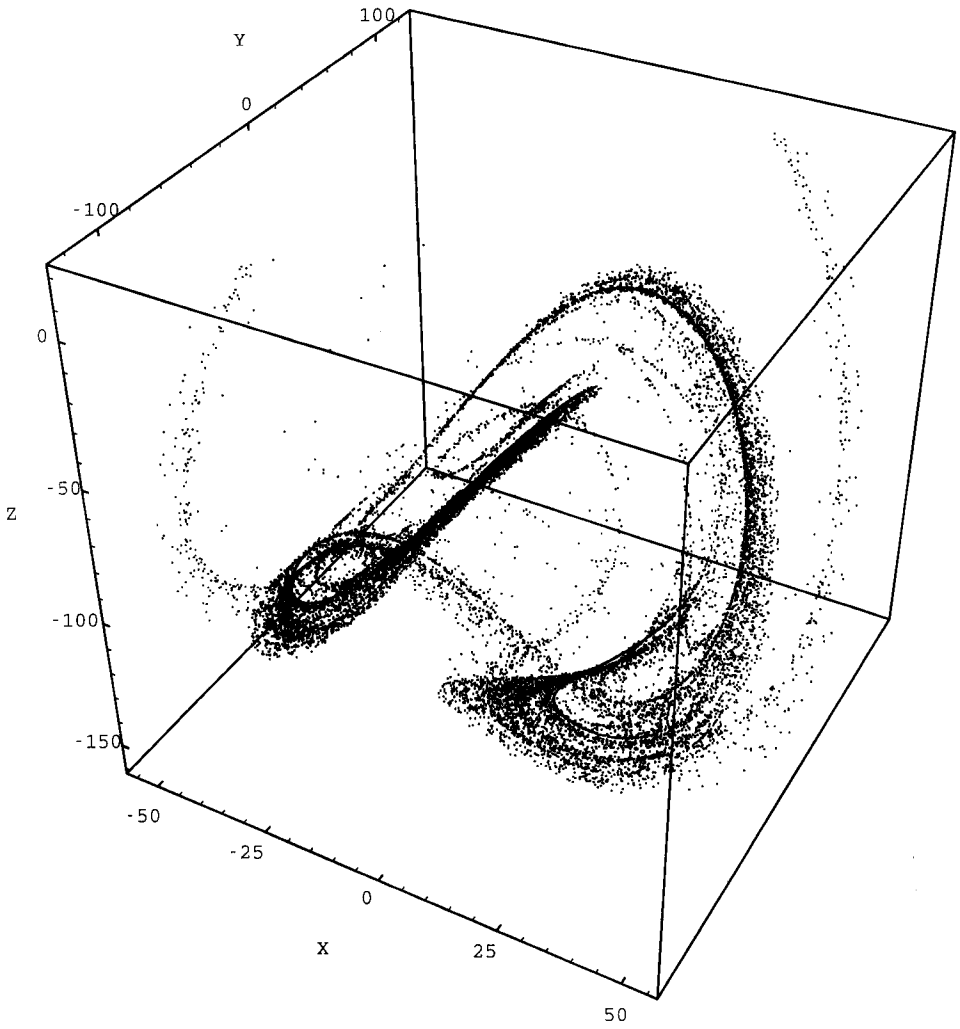

Fig. 6. The 3-D phase portrait of the period map of the "blinking Lorenz" system for switching period $p = 0.18$. The number of samples is $n = 20000$.

5.4. *"Blinking Lorenz"*

Let us consider the vector field

$$\mathbf{v}(x, y, z) = \begin{bmatrix} \sigma(y - x) \\ rx - y - xz \\ -bz + xy \end{bmatrix}, \qquad (39)$$

where $\sigma = 10$, $b = \frac{8}{3}$, $r = 28$, and linear involutory diffeomorphism

$$G(x, y, z) = (x, y, -z). \qquad (40)$$

Then the vector field $\mathbf{w} = G_*\mathbf{v}$ has the form

$$\mathbf{w}(x, y, z) = \begin{bmatrix} \sigma(y - x) \\ rx - y + xz \\ -bz - xy \end{bmatrix}.$$

The attractor of the system $\dot{X} = \mathbf{v}(X)$ ($X = (x, y, z)$) — the Lorenz attractor [Lorenz, 1963] — is plotted in Fig. 5, the attractor of the system $\dot{X} = \mathbf{w}(X)$ is its mirror image with respect to the x–y plane. And finally the attractor of period mapping P of the system (4), for switching period $p = 0.18$ is plotted in Fig. 6. Lyapunov exponents for this attractor are $\lambda_1 \doteq 1.377$, $\lambda_2 \doteq -0.864$, $\lambda_3 \doteq -5.433$ (evaluated using 10^5 iterations), which gives, using the Kaplan–Yorke conjecture [Kaplan & Yorke, 1979], the dimension estimate $D = 2 + (\lambda_1 + \lambda_2)/|\lambda_3| \doteq 2.094$ for the discrete-time system and 3.094 for the continuous-time system. Compared to the same estimate of the dimension of the original Lorenz attractor ($D = 2.062$) gives that the procedure of "blinking" has increased the dimension by slightly more than 1.

The original system (39) has a strange attractor above the x–y plane. The map (40) corresponds to a symmetry with respect to the x–y plane. The averaged system $\mathbf{X} = (\mathbf{v} + \mathbf{w})/2$ is linear with the origin being a saddle steady state with one unstable and two stable directions. Thus for small switching period p the blinking system has an attractor whose diameter becomes large as $p \to 0$. When changing p, there are intervals when the attractor of the period map is a single point, while for other values of p the attractor is more complex. This is illustrated in Fig. 7 where for different values of the switching period p and random initial conditions the x-projection of the attractor is plotted. The intervals of p where the attractor is a single point are located approximately around integer multiples of $T_0 = 2\pi/\omega \approx 0.616$ where ω is the imaginary part of the complex eigenvalue of the Jacobi matrix at the nonzero steady point of the Lorenz system.

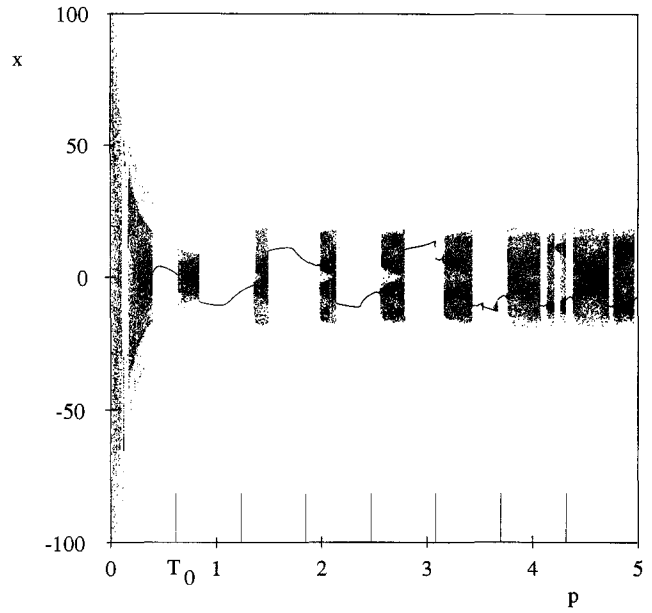

Fig. 7. The x-projection of the attractor of the period map for the "blinking Lorenz" system is plotted for various values of the switching period p. For certain intervals of p located approximately around integer multiples of T_0 (see text) the attractor is a single point while for other values chaos persists.

The largest Lyapunov exponent λ_1 and the sum of the two largest Lyapunov exponents $\lambda_1 + \lambda_2$ of the period map as a function of p is plotted in Fig. 8. For $p \to 0$, λ_1 and λ_2 are proportional to p as the period map approaches identity. For certain intervals of p, λ_1 is negative which corresponds to the single-point attractor of the period map shown in Fig. 7 or equivalently to the stable limit cycle of the continuous time system. For certain values of p, λ_1 is positive indicating chaos. Note that inside the "mainly chaotic" region $(0.18; 0.40)$ the sum $\lambda_1 + \lambda_2$ changes

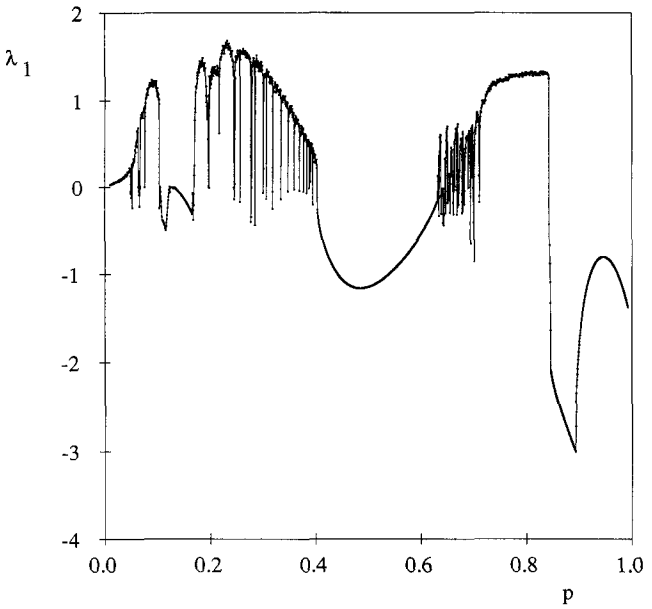

(a)

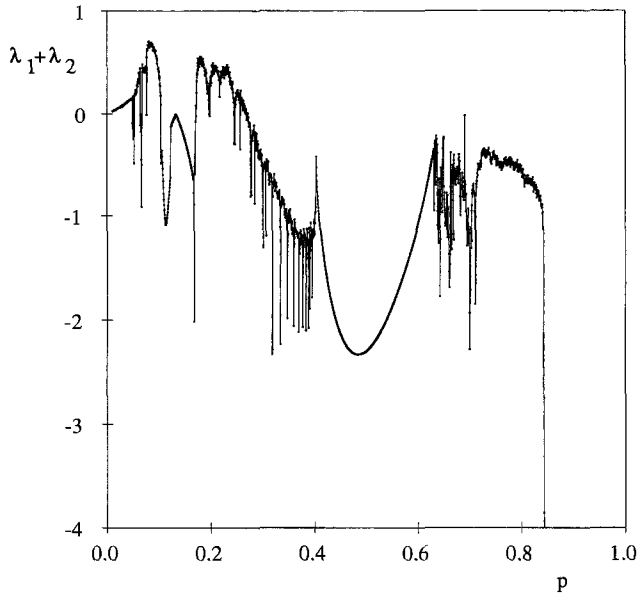

(b)

Fig. 8. (a) the largest Lyapunov exponent and (b) the sum of the two largest Lyapunov exponents of the period map of the "blinking Lorenz" system as a function of the switching period p.

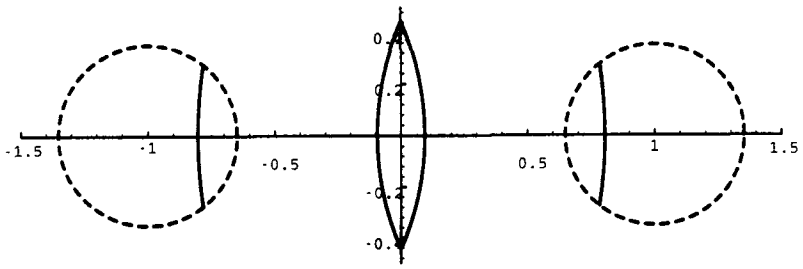

Fig. 9. Typical fixed points of the "blinking vortex" system (here $p = 1$). Rotation for more than 360° is indicated by a dashed line.

the sign (for $p \approx 0.27$) meaning the decreasing of the dimension estimate below 2.

5.5. *"Blinking vortex"*

The well-known blinking vortex flow, see for example [Ottino, 1989], can be described using the system (4) as follows:

Let us have

$$\mathbf{v}(x, y) = \left[\frac{-y}{(x-1)^2 + y^2}, \frac{x-1}{(x-1)^2 + y^2}\right].$$

This vector field $\mathbf{v}$ determines the flow of a single vortex located at the point (1, 0).

Let us put

$$G_1(x, y) = (-x, -y),$$

i.e. G_1 is the symmetry with respect to the origin, and

$$G_2(x, y) = (-x, y),$$

i.e. G_2 is the symmetry with respect to the y-axis.

Then the vector field $\mathbf{w}_1 = G_{1*}\mathbf{v}$ has the form

$$\mathbf{w}_1(x, y) = \left[\frac{-y}{(x+1)^2 + y^2}, \frac{x+1}{(x+1)^2 + y^2}\right]$$

and the vector field $\mathbf{w}_2 = G_{2*}\mathbf{v}$ has the form

$$\mathbf{w}_2(x, y) = \left[\frac{y}{(x+1)^2 + y^2}, \frac{-x-1}{(x+1)^2 + y^2}\right].$$

The system (4), where $\mathbf{w} = \mathbf{w}_1$, describes the system with two co-rotating point vortices and the system (4), where $\mathbf{w} = \mathbf{w}_2$, describes the system with two counter-rotating point vortices, the second vortex located at the point $(-1, 0)$. In the following paragraph we shall consider the co-rotating case.

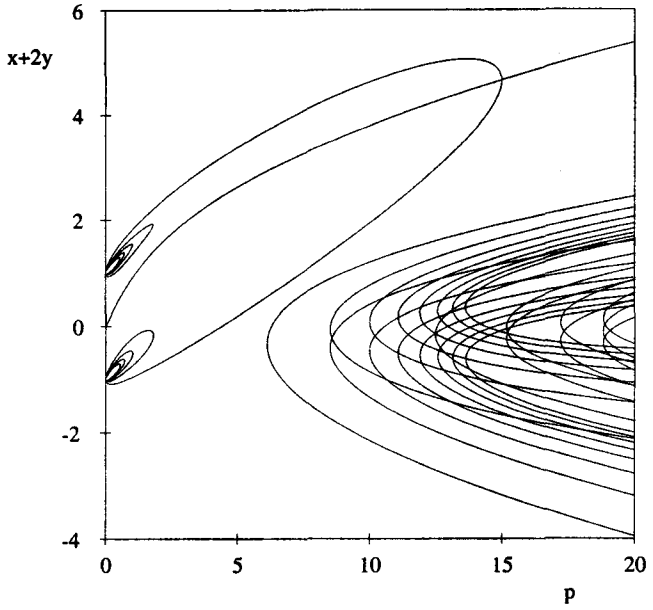

Fig. 10. The bifurcation diagram of the period map of the "blinking vortex" system. The projection $x + 2y$ versus p is chosen to avoid degeneracy due to symmetries present in the system. Two nests of branches of steady points for small p (only the 4 outermost are depicted here), the large branch and numerous branches for large p can be seen.

Fixed points of period mapping P.

With respect to the relation (10), the period mapping P has two kinds of fixed points. The fixed point of P is a fixed point of H or fixed point of P corresponds to a 2-periodic orbit of H. The situation is illustrated in Fig. 9, where $\hat{X} = H(\hat{X}) = P(\hat{X})$, $\hat{Y} = \varphi^p(\hat{X}) = G(\hat{X})$, see the relation (11). Further $H(X_1) = X_2$ and $H(X_2) = X_1$, i.e. $Y_1 = \varphi^p(X_1) = G(X_2)$ and $Y_2 = \varphi^p(X_2) = G(X_1)$, see the relation (25).

The fixed points of H lie on the y-axis while the other fixed points of P corresponding to the 2-periodic orbits of H do not lie on the y-axis.

The dependence of the fixed points of P on the switching period p, i.e. the bifurcation diagram, is plotted in Fig. 10. Fixed points of the period map of the blinking vortex flow system lie on 1-D curves in the 3-D space x-y-p. Due to symmetries present in the system some curves coincide in both the p-x and the p-y projections. To get the complete picture the projection $x + 2y$ versus p is chosen in Fig. 10.

In Appendix B six different qualitative cases of the blinking vortex flow system are given according to the strength a_i and the sense of rotation of the two vortices. The first integral of the averaged system (for $p \to 0$) is shown to be

$$r_1^{a_1} r_2^{a_2} = \text{const}\,. \tag{41}$$

6. Conclusion

Periodic flow reversal used in engineering has been studied on a mathematical basis. Periodic solutions of the non-autonomous system have been shown to originate in fixed points (either isolated or non-isolated) of the involutory diffeomorphism describing the geometrical reversion. Detailed numerical study of both dissipative ("blinking nodes", "blinking cycles", "blinking Lorenz") and conservative ("blinking vortex") systems has shown that the method of blinking can be used to originate and control of chaos. For systems with a single limit cycle, the blinking can be used to synchronize the system, to change the period, to establish bistability and to initiate chaotic motion in a defined way. For systems already possessing a chaotic attractor the method of blinking can be used either to stabilize the motion at a fixed point or to enhance the complexity (to increase the Lyapunov exponent and the Hausdorff dimension of the attractor).

Acknowledgments

This work was supported by the grant 201/94/1111 of the Czech Grant Agency. The computation was done at the Prague Institute of Chemical Technology, in the Computing Center of the Czech Technical University Prague and in the Supercomputing Center at the Charles University Prague.

References

Chen, G. & Dong, X. [1993] "From chaos to order — perspectives and methodologies in controlling chaotic nonlinear dynamical systems," *Int. J. Bifurcation and Chaos* **3**, 1363–1409.

Chirikov, B. V. [1979] "A universal instability of many-dimensional oscillator systems," *Phys. Rep.* **52**, 263.

Kaplan, J. & Yorke, J. A. [1979] "Chartie behaviour of multidimensional difference equations", *Functional Differential Equations and Approximations of Fixed Points*, eds. Peitgen, H. O. and Walther, H. O. (Springer, Heidelberg, New York).

Klíč, A. & Řeháček, J. [1994] "On systems governed by two alternating vector fields," *Appl. of Math.* **39**, 57–64.

Lorenz, E. N. [1963] "Deterministic nonperiodic flow," *J. Atmos. Sci.* **20**, 130.

Matveev, N. M., Nosov, S. L. & Pokrovskij, A. N. [1978] "K voprosu o principe usrednenija (to problem of averaging principle)," *Differencialnije uravnenija* **XIV**, 371–373.

Ogorzalek, M. J. [1993] "Taming chaos — Part II: Control," *IEEE Trans. on Circ. Sys. I* **40**, 700–706.

Ottino, J. M. [1989] *The Kinematics of Mixing, Stretching, Chaos and Transportations* (Cambridge University Press).

Palmer, K. J. [1984] "Exponential dichotomies and transversal homoclinic points," *J. Diff. Eq.* **55**, 225–256.

Pokorný, P. [1995] *Easyplot* (Pokorný Praha).

Pokorný, P. [1995] *Numerical Library Easynum* (Pokorný Praha).

Pokorný, P. [1995] *Xpplot* (Pokorný Praha).

Řeháček, J., Kubíček, M. & Marek, M. [1992] "Modelling of a tubular catalytic reactor with flow reversal," *Chem. Engng Sci.* **47**, 2897–2902.

Shinbrot, T., Grebogi, C., Ott, E. & Yorke, J. A. [1993] "Using small perturbations to control chaos," *Nature* **363**, 411–417.

Appendix A
Palmer's Theorem

Theorem [Palmer, 1984]. Let $\mathcal{E}$, $\mathcal{F}$ be Banach spaces and let

$$F : \mathcal{E} \times R \to \mathcal{F}, \quad (x, \mu) \in \mathcal{E} \times R$$

be a C^2 mapping defined on a neighborhood of $(x_0, 0)$ such that $F(x_0, 0) = 0$ and

$$L = F_x(x_0, 0)$$

is Fredholm with index zero. Then if:

(i) $F(x, 0) = 0$ for $x \in \mathcal{M}$ a C^2 submanifold of $\mathcal{E}$ containing x_0 with $\mathcal{N}(L)$ as tangent space at x_0. (More precisely: $T_{x_0}\mathcal{M} = x_0 \oplus \mathcal{N}(L)$.)

(ii) $Lx = -F_\mu(x_0, 0)$ has a solution u, i.e. $F_\mu(x_0, 0) \in \mathcal{R}(L)$.

(iii) $y \in \mathcal{N}(L)$ and $\{F_{xx}(x_0, 0)u + F_{\mu x}(x_0, 0)\}y \in \mathcal{R}(L) \Leftrightarrow y = 0$, then there is a neighborhood of x_0 in $\mathcal{E}$ such that for μ sufficiently small the equation $F(x, \mu) = 0$ has a solution $x(\mu)$ in this neighborhood which is unique when $\mu \neq 0$. Moreover, $x(0) = x_0$, $x(\mu)$ is C^1 and when $\mu \neq 0$, $F_x(x(\mu), \mu)$ is invertible.

(Remark: Note that if L is a linear operator, we denote by $\mathcal{N}(L)$ its kernel and by $\mathcal{R}(L)$ its range.)

Appendix B
Averaged "Blinking Vortex" System

We investigate a conservative, non-autonomous, 2-dimensional dynamical system with continuous time, whose dynamics switches with period $2p$ between two vector fields. For $0 \leq t < p$

$$\frac{\mathrm{d}z}{\mathrm{d}t} = 2i\omega_1(z - z_1) \tag{B.1}$$

and for $p \leq t < 2p$

$$\frac{\mathrm{d}z}{\mathrm{d}t} = 2i\omega_2(z - z_2)\,,$$

where z is the complex state variable, z_1 and z_2 are two complex constants (two centers of rotation), ω_1 and ω_2 are two angular velocities, that may or may not depend on z. We shall assume that ω_1 and ω_2 are real (if they are complex, the system is not conservative).

If ω_1 and ω_2 do not depend on z, we have a composition of two rotations which is again a rotation (the special case $\omega_1 = -\omega_2$ is a transition).

Let us consider the case when

$$\omega_1 = \frac{a_1}{|z - z_1|^2} \tag{B.2}$$

and

$$\omega_2 = \frac{a_2}{|z - z_2|^2}\,,$$

where $|z|$ denotes the absolute value of z; a_1 and a_2 are real constants and their signs determine one of the following six cases:

Table 1. Different types of "blinking vortex" system

1	$a_1 = 0$ and $a_2 = 0$	identity
2	$a_1 = 0$ and $a_2 \neq 0$ or $a_2 = 0$ and $a_1 \neq 0$	single rotation
3	$a_1 a_2 > 0$	co-rotation
4	$a_1 = a_2 \neq 0$	exact co-rotation
5	$a_1 a_2 < 0$	counter-rotation
6	$a_1 = -a_2 \neq 0$	exact counter-rotation

First, we will investigate the limit $p \to 0$. This results in the autonomous system

$$\frac{\mathrm{d}z}{\mathrm{d}t} = ia_1\frac{z - z_1}{|z - z_1|^2} + ia_2\frac{z - z_2}{|z - z_2|^2}\,. \tag{B.3}$$

Let us investigate the distance r_1 (r_2 respectively) between the state point z and the center z_1 (z_2 respectively). The time evolution $\dot{r} = \frac{\mathrm{d}r}{\mathrm{d}t}$ of the absolute value r of a complex number z can be expressed using

$$z = re^{i\varphi}$$

$$\log z = \log r + i\varphi$$

$$\frac{\dot{z}}{z} = \frac{\dot{r}}{r} + i\dot{\varphi}$$

$$\dot{r} = r\mathrm{Re}\frac{\dot{z}}{z};$$

using

$$z - z_1 = r_1 e^{i\alpha_1}$$

and

$$z - z_2 = r_2 e^{i\alpha_2}$$

we have

$$\begin{aligned}
\dot{r_1} &= r_1\mathrm{Re}\frac{(z - z_1)^{\cdot}}{z - z_1} \\
&= r_1\mathrm{Re}\frac{(z)^{\cdot}}{z - z_1} \\
&= r_1\mathrm{Re}\left(ia_1\frac{1}{|z - z_1|^2} + ia_2\frac{z - z_2}{|z - z_2|^2(z - z_1)}\right) \\
&= r_1\mathrm{Re}\left(ia_2\frac{z - z_2}{|z - z_2|^2(z - z_1)}\right) \\
&= -\frac{r_1}{r_2^2}a_2\mathrm{Im}\frac{z - z_2}{z - z_1} \\
&= -\frac{a_2}{r_2}\sin(\alpha_2 - \alpha_1)
\end{aligned}$$

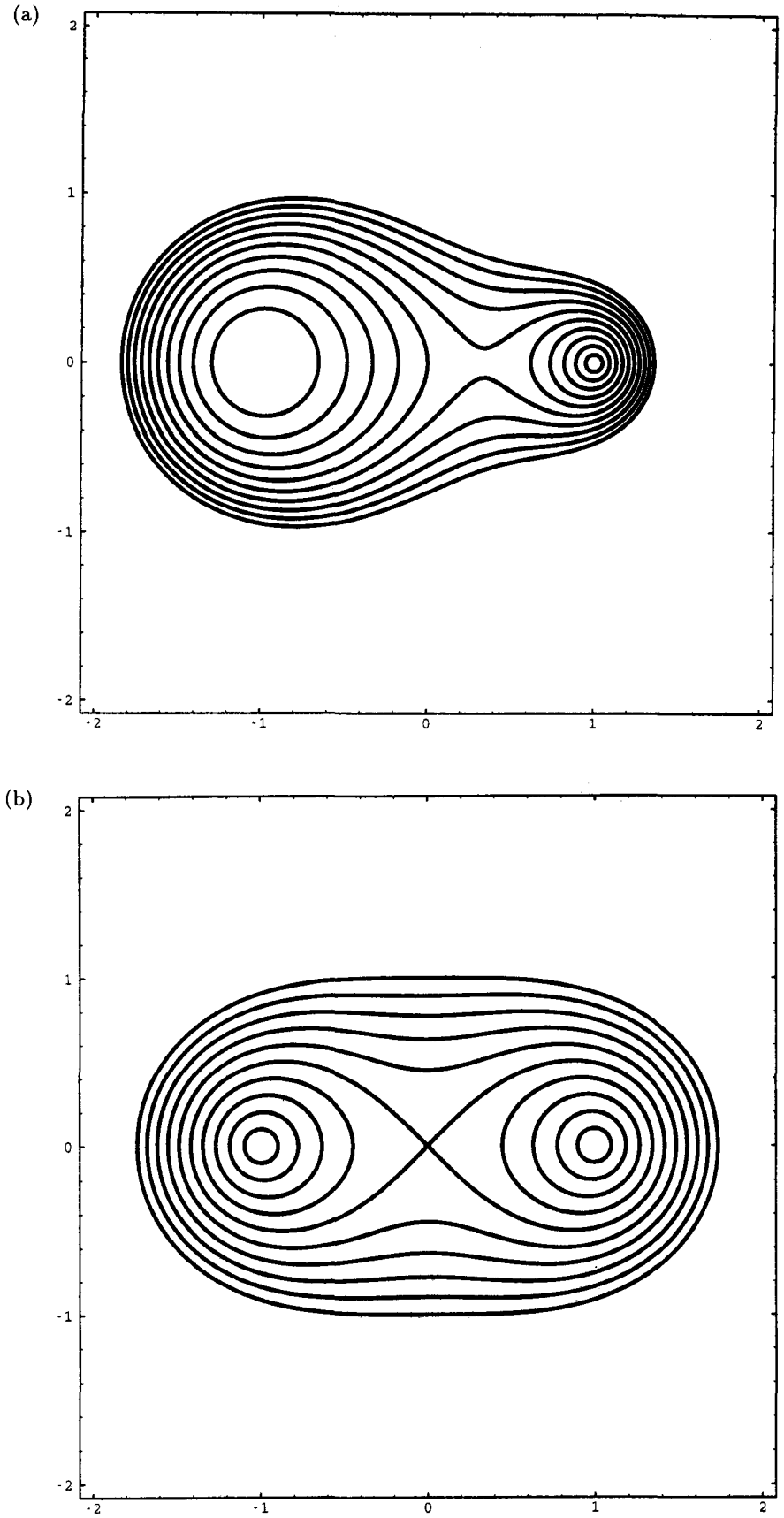

Fig. 11. Trajectories of the averaged "blinking vortex" system constructed as level lines of the first integral $I(z) = |z - z_1|^{a_1}|z - z_2|^{a_2}$. (a) co-rotation, (b) exact co-rotation, (c) counter-rotation, (d) exact counter-rotation.

(c)

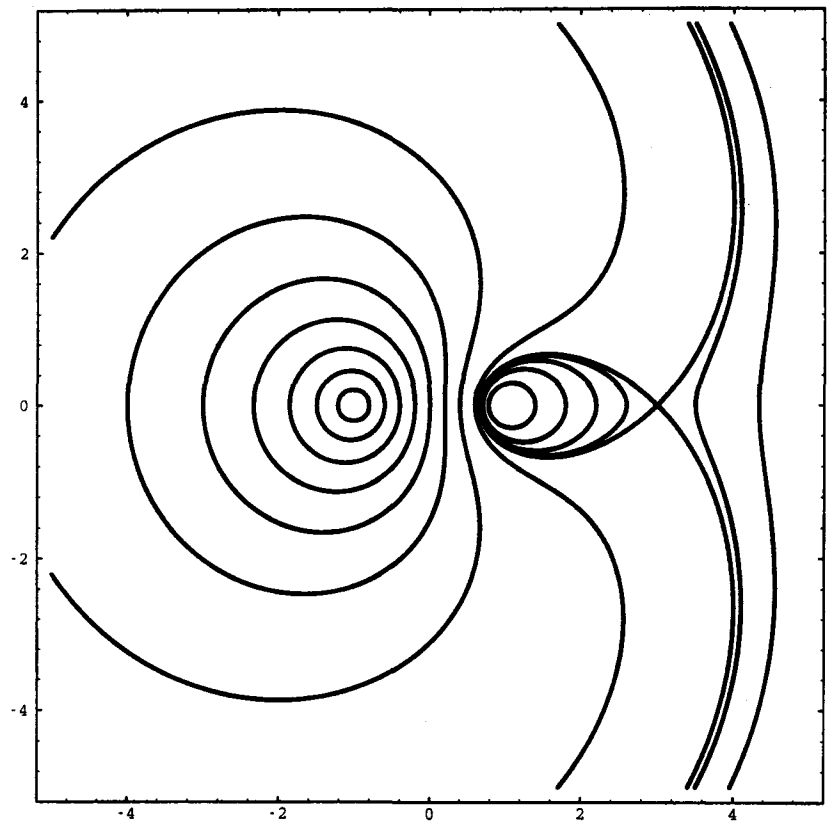

(d)

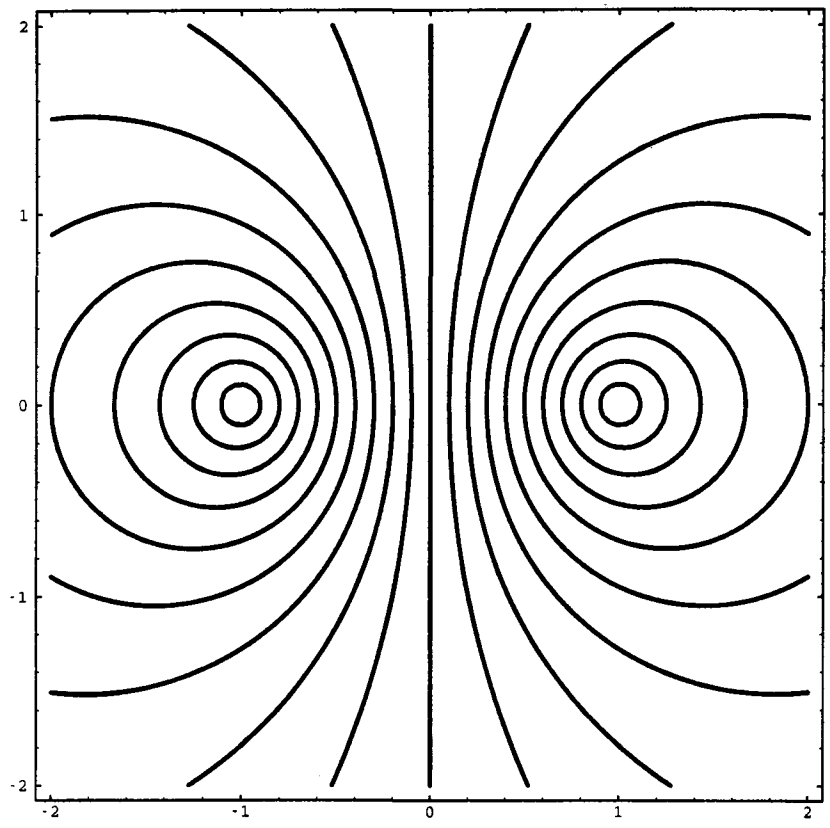

Fig. 11. (*Continued*)

and similarly

$$\dot{r_2} = -\frac{a_1}{r_1}\sin(\alpha_1 - \alpha_2)\,.$$

Combining these two results gives

$$a_1\frac{\dot{r_1}}{r_1} + a_2\frac{\dot{r_2}}{r_2} = 0$$

$$\log(r_1^{a_1} r_2^{a_2}) = \text{const}$$

$$r_1^{a_1} r_2^{a_2} = \text{const} \tag{B.4}$$

Specially for $a_1 = a_2$ (exact co-rotation)

$$r_1 r_2 = \text{const}$$

and for $a_1 = -a_2$ (exact counter-rotation)

$$\frac{r_1}{r_2} = \text{const}\,.$$

Result (B.4) is the first integral of motion of Eq. (B.3). Level lines of $I(z) = |z-z_1|^{a_1}|z-z_2|^{a_2}$ for different initial conditions are shown in Figs. 11(a)–11(d) for poles $z_1 = -1$ and $z_2 = 1$.

In Fig. 11(a) the case of co-rotation is depicted ($a_1 = 2$, $a_2 = 1$). It shows the trajectories of the system in the z-plane with 3 singular points: the poles z_1 and z_2 and a saddle point z_S. The poles are surrounded by nearly circular trajectories with high frequency. The sense of rotation around both poles is the same and so are the values of the integral $I(z_1) = I(z_2) = 0$. The saddle point has coordinates

$$z_S = \frac{a_1 z_2 + a_2 z_1}{a_1 + a_2} \tag{B.5}$$

which is $z_S = 1/3$ for Fig. 11(a).

Figure 11(b) shows trajectories for exact co-rotation ($a_1 = a_2 = 1$). The saddle point has moved to $z_S = 0$.

Figure 11(c) shows trajectories for counter-rotation ($a_1 = -2$, $a_2 = 1$). The poles are again surrounded by small nearly circular trajectories. The sense of rotation around one pole is opposite to the sense of rotation around the other pole and also the integral differs: $I(z_1) = \infty$, $I(z_2) = 0$. The saddle point has moved outside the segment between z_1 and z_2. For distant initial condition $|z(0)| \gg |z_1 - z_2|$ the trajectory is a large cycle (similar to that for co-rotation) with the sense of rotation given by the "stronger" pole (that with larger absolute value of a_i).

Figure 11(d) shows trajectories for exact counter-rotation ($a_1 = -1$, $a_2 = 1$). The saddle point has moved to infinity and the phase portrait is symmetrical around the axis of the segment between the poles. This axis divides the entire phase space to two regions with $I > 1$ and $I < 1$.

Now let us investigate what happens if we lift the constraint $p \to 0$. The parameter p is the time for which the system (B.1) rotates around one of the two poles. For small $p > 0$ the dynamics will change qualitatively for those trajectories with rapid rotation. From (B.2) we can see that the rapid motion appears in the vicinity of poles, namely in distances $r < r_C$. We can find the scaling of the critical distance r_C from the pole, beyond which the trajectory for $p > 0$ will be similar to that for $p \to 0$. From

$$T \propto \frac{1}{\omega} \propto r^2$$

we have

$$r_C \propto \sqrt{p}\,.$$

This means that for $p > 0$ there may appear regions of radius $r_C \propto \sqrt{p}$ around the poles with qualitatively different dynamics. Numerical observations support this prediction.